Radiation dose and image quality for paediatric interventional cardiology

2008 Phys. Med. Biol. 53 4049

(http://iopscience.iop.org/0031-9155/53/15/003)

IOP PUBLISHING PHYSICS IN MEDICINE AND BIOLOGY

Phys. Med. Biol. **53** (2008) 4049–4062 doi:10.1088/0031-9155/53/15/003

Radiation dose and image quality for paediatric interventional cardiology

E Vano[1], C Ubeda[2], F Leyton[3] and P Miranda[4]

[1] Radiology Department, Medicine School, Complutense University and San Carlos University Hospital, 28040 Madrid, Spain
[2] Clinical Sciences Department, Faculty of the Science of Health, Tarapaca University, 18 de Septiembre 2222, Arica, Chile
[3] Institute of Public Health of Chile, Marathon 1000, Nunoa, Santiago, Chile
[4] Hemodynamic Department, Cardiovascular Service, Luis Calvo Mackenna Hospital, Avenida Antonio Varas 360, Providencia, Santiago, Chile

E-mail: eliseov@med.ucm.es

Received 23 May 2008, in final form 14 June 2008
Published 8 July 2008
Online at stacks.iop.org/PMB/53/4049

Abstract

Radiation dose and image quality for paediatric protocols in a biplane x-ray system used for interventional cardiology have been evaluated. Entrance surface air kerma (ESAK) and image quality using a test object and polymethyl methacrylate (PMMA) phantoms have been measured for the typical paediatric patient thicknesses (4–20 cm of PMMA). Images from fluoroscopy (low, medium and high) and cine modes have been archived in digital imaging and communications in medicine (DICOM) format. Signal-to-noise ratio (SNR), figure of merit (FOM), contrast (CO), contrast-to-noise ratio (CNR) and high contrast spatial resolution (HCSR) have been computed from the images. Data on dose transferred to the DICOM header have been used to test the values of the dosimetric display at the interventional reference point. ESAK for fluoroscopy modes ranges from 0.15 to 36.60 μGy/frame when moving from 4 to 20 cm PMMA. For cine, these values range from 2.80 to 161.10 μGy/frame. SNR, FOM, CO, CNR and HCSR are improved for high fluoroscopy and cine modes and maintained roughly constant for the different thicknesses. Cumulative dose at the interventional reference point resulted 25–45% higher than the skin dose for the vertical C-arm (depending of the phantom thickness). ESAK and numerical image quality parameters allow the verification of the proper setting of the x-ray system. Knowing the increases in dose per frame when increasing phantom thicknesses together with the image quality parameters will help cardiologists in the good management of patient dose and allow them to select the best imaging acquisition mode during clinical procedures.

Abbreviations

BG	background
BS	backscatter
CI	cine
CNR	contrast-to-noise ratio
CO	contrast
DAP	dose–area product
DDO	dynamic density optimization
DICOM	digital imaging and communications in medicine
ESAK	entrance surface air kerma
FOM	figure of merit
FOV	field of view
HCSR	high contrast spatial resolution
HD	high dose
II	image intensifier
KAP	kerma–area product
LD	low dose
MD	medium dose
PMMA	polymethyl methacrylate
ROI	region of interest
SD	standard deviation
SNR	signal-to-noise ratio

1. Introduction

It is known that medical exposure is at present the main source of radiation doses to the population, in particular computed tomography and interventional procedures (UNSCEAR 2000). Fluoroscopically guided cardiac procedures in paediatrics require special attention considering the increase in frequency and the high radiosensitivity of the patients (Bacher *et al* 2005, Wagner 2006).

X-ray systems used for interventional procedures are quite difficult to evaluate due to their many setting options and operational modes. Sometimes, interventionists do not have clear criteria to select the different operation modes. Thus, the characterization of the systems in dose and image quality using test objects offers a set of useful data to help cardiologists to select the most appropriate operation modes for the different procedures and patient sizes.

Some studies involving the evaluation of x-ray systems used for cardiac procedures in adults have been published (Tsapaki *et al* 2004a, 2004b, Vano *et al* 2005, Balter *et al* 2008), but these reports are scarce in paediatric cardiology (Martinez *et al* 2007). Papers analysing the correlation between phantom (or patient) doses and image quality are practically non-existent for the paediatric systems used in interventional cardiology.

During the characterization of x-ray and imaging systems, some basic information about the modes of operation can be obtained: dose rates for fluoroscopy, dose per cine (CI) frame, doses for different field of views (FOVs), etc, and how these values change with the thickness of the phantom, to later correlate the results with the size of the patients and the different angulations of the C-arm. All these dose values need to be balanced with the image quality obtained in the different operation modes. Results of these measurements should be reported to the cardiologists to help in the optimization of clinical procedures.

The initial settings of the x-rays systems, which influence patient dose and image quality, are sometimes customized in different ways by the service engineers, depending on the clinical procedures to be undertaken and the particular preferences of the interventionists.

The characterization of dose and image quality of the x-ray and imaging systems helps cardiologists to select the best protocols (new born, infant or child in our case) and operation modes to have enough image quality to guide and document the procedures. This characterization using different polymethyl methacrylate (PMMA) thicknesses and test objects is especially important in paediatric settings considering the dramatic variation in size of the patients.

This evaluation of the x-ray and imaging systems is relevant during the commissioning of the equipment in cardiac laboratories and the interpretation of the results should be part of the training programmes in quality assurance and radiation protection of the cardiologists (training required by European Directive 97/43/EURATOM (EC 1997) and recommended in other international programmes such as the IAEA ARCAL project RLA/9/057 (IAEA 2007)).

Sometimes, visual evaluation of the images is not enough to decide whether the default settings of the x-ray systems are the best ones for the different patient sizes or if some changes may be introduced to obtain a similar image quality with lower patient doses. Numerical evaluations using test object images will help to optimize these settings.

This paper presents the methodology and results of the characterization of a biplane x-ray system set for paediatric cardiac procedures. Detailed results on entrance surface air kerma (ESAK) measured on PMMA phantoms and image quality for the most common operation modes have been evaluated using a test object and different thicknesses equivalent to the full range of paediatric patients. In addition, the correspondence between the cumulative dose values reported by the x-ray system and the measured ones is also reported for typical paediatric thicknesses.

2. Materials and methods

We use the more familiar quantity of dose–area product (DAP), equivalent to air kerma–area product (KAP) proposed by the International Commission on Radiological Units (ICRU 2005). The quantity cumulative dose, referred to in the standard IEC 60601-2-43 (IEC 2000), is equivalent to the incident air kerma without backscatter (BS) (ICRU 2005) at the interventional reference point. This point is intended to be representative of the position of the patient's skin at the entrance site of the x-ray beam during an interventional procedure. For fluoroscopic systems with an isocentre, the interventional reference point is located along the central ray of the x-ray beam at a distance of 15 cm from the isocentre in the direction of the focal spot (IEC 2000).

The evaluated x-ray system was a biplane Siemens Axiom Artis BC (equipped with image intensifier (II)) (Siemens 2008). The system includes internal selectable post-processing software called dynamic density optimization (DDO), which allows the improvement of image quality using online harmonization of the contrast. In our measurements, the standard DDO was maintained at its default value during fluoroscopy modes (40%). For CI acquisition, the selected DDO value was zero. Routine clinical protocols use DDO from 0 to 60%. Information on the criteria to use this post-processing is still scarce and different settings are found in different centres requiring more research in the future.

Spectral shaping copper filters are automatically inserted in the x-ray beam depending on patient absorption to reduce skin dose. Some additional technical and operation details are included in table 1.

Table 1. Technical details of the x-ray system Siemens Axiom Artis BC and the evaluated operation modes.

Generator of 100 kW at 100 kV
Three available fluoroscopy modes: low, medium and high dose
Three evaluated exam protocols for paediatrics: newborn, infant and child
All fluoroscopy modes configured in pulsed fluoroscopy with 15 pulses s^{-1}
Cine mode at 30 frames s^{-1}
Three available fields of view: 16, 22 and 33 cm
Additional filters: from 0.1 to 0.9 mm Cu
Virtual collimation available
Isocentre-to-floor distance 107 cm
Focus-to-isocentre distance 76 cm

The system is equipped with an ionization transmission chamber integrated into the collimator housing to measure DAP values. Different dosimetric displays can be configured for live fluoroscopy and for fluoroscopy pause. During fluoroscopy, DAP and incident air kerma at the interventional reference point rates are displayed on the in-room monitors.

The system has been characterized using the protocols agreed during the DIMOND and SENTINEL European programmes (Faulkner 2001, Vano *et al* 2005, Faulkner *et al* 2008, Simon *et al* 2008) and adapted in our case to paediatric procedures. PMMA plates of dimensions 25 cm × 25 cm × 1 cm have been employed, building thicknesses of 4, 8, 12, 16 and 20 cm simulating the full range of equivalent paediatric patients. The ratio between the PMMA and the patient chest thickness can be considered to be approximately 1.5 (Rassow *et al* 2000). A test object (Leeds TOR 18-FG)[5] was positioned at the isocentre and at the middle of the PMMA thickness during all measurements, thus providing the best geometry to simulate real clinical conditions.

The Leeds TOR-18FG is designed to provide an ongoing check of imaging performance for fluoroscopy systems. The object contains a set of 14 line-pair groups for high contrast spatial resolution (HCSR) (with a limit of 5 line pairs mm^{-1}) and 18 circles (11 mm diameter) for low-contrast threshold evaluation. This test object has been adopted in the aforementioned European DIMOND protocol (Faulkner 2001) for the initial characterization and constancy checks of these x-ray systems.

A solid-state detector Unfors Xi (model 8201010-A) with a measurement probe (model 82020030-AXi)[6] in contact with the PMMA plates was used to measure incident air kerma. To facilitate the comparison of our results with other measurements of ESAK, a BS factor 1.3 has been used (ICRU 2005). The Unfors Xi detector was positioned at the entrance of the PMMA, outside of the automatic exposure control to avoid influence on the radiographic technique adjusted by the system. Measurements were made without removing the antiscatter grid. Image quality has been evaluated simultaneously with dose measurements. The Unfors Xi detector was duly calibrated, traceable to official calibration laboratories[7]. Figure 1 shows the experimental arrangement with detector, PMMA phantom and test object.

The test object, and especially the line-pair test pattern for HCSR, increases the dose rate at the entrance to the PMMA due to the automatic exposure control of the system. However, this experimental condition was maintained throughout the experiment and may be considered as a constant slight increase in patient thickness or equivalent to the effect of the iodine contrast

[5] http://www.leedstestobjects.com/products/tor/product-tor-18fg.htm, Leeds, UK.
[6] http://www.unfors.com/products.php?catid = 19
[7] Unfors instruments AB. Certificate N°:142527–20071031. Sweden.

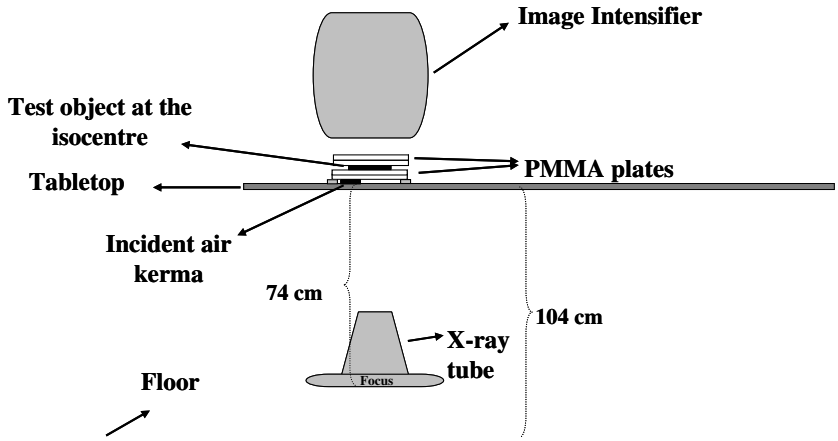

Figure 1. Experimental arrangements to measure incident air kerma and image quality using a PMMA slab phantom.

media during clinical procedures. The relative increases in entrance doses have been measured in previous similar experiments and resulted in percentages of 15–20% (Vano *et al* 2005).

For a PMMA thickness of 4 cm and with the test object at the isocentre, the floor-to-tabletop distance was 104 cm. The table-to-solid-state detector Unfors Xi distance was 1 cm. The tabletop-to-isocentre distance was 3 cm, and the focus-to-detector of x-rays Unfors Xi distance was 74 cm. For 8, 12, 16 and 20 cm of PMMA, this distance was decreased to 72, 70, 68 and 66, respectively, to maintain the test object at the isocentre (the table was moved down 2 cm when 4 cm of PMMA was added). The II was always kept 5 cm from the top side of the PMMA slab (also to simulate typical clinical working conditions).

Due to the many measurements made (for 4, 8, 12, 16 and 20 cm of PMMA) for all the fluoroscopy and acquisition modes and to avoid errors in dose measurements, images of the test object (to evaluate image quality) were recorded simultaneously with the dose measurements.

The acquisition and recording format of the images, together with the visualization (monitor and viewer software), have a strong influence on the results of image quality evaluation, but all these factors have been maintained as constant during the full process of evaluation. The used x-ray system has the capability to archive short sequences of fluoroscopy runs in DICOM (digital imaging and communications in medicine) format, allowing numerical analysis of the image quality of individual fluoroscopy frames.

In the system evaluated, it was possible to archive DICOM images in 1024 × 1024 pixels and 12 bits or in 512 × 512 pixels and 8 bits, if the CD-ROMs are burned at the workstation of the x-ray system. If the images are transferred to another workstation of the network, they are automatically compressed to 512 × 512 pixels and 8 bits, according to a site-specific system configuration. Because this is at present the most common format used in cardiology, image quality was evaluated on this reduced matrix size format.

Osiris software, version 4.18,[8] was used to evaluate the images (CI and fluoroscopy frames) with an IBM Corporation Intel[R] Pentium[R] M processor 1.73 GHz, 198 MHz, 760 MB of RAM (with a screen mode of 1024 × 768 pixels, IBM ThinkPad LCD mobile Intel[R] 915GMGMS)[9] . The numerical evaluation of image quality was always done on three

[8] http://www.sim.hcuge.ch/osiris/01 Osiris Presentation EN.htm.
[9] http://www.ibm.com/es/

images (numbers 5, 8 and 10 of the series), and mean values and standard deviations (SDs) were reported. The first two to three images exhibit varying image quality until the automatic exposure control stabilizes the radiographic technique of the generator.

Image quality was evaluated by analysing the low-contrast circles and the HCSR groups. A numerical analysis of the signal-to-noise (SNR), figure of merit (FOM), contrast (CO) and contrast-to-noise (CNR) (Massoumzadeh *et al* 1998, Gagne *et al* 2003) has been done. These numerical parameters are defined as

$$\mathrm{SNR} = \frac{[\mathrm{BG} - \mathrm{ROI}]}{\sqrt{\frac{\left(\mathrm{STD}_{\mathrm{ROI}}^2 + \mathrm{STD}_{\mathrm{BG}}^2\right)}{2}}} \tag{1}$$

where

- BG is the background value, in our case the mean value of the pixel content in the region of interest (ROI) selected from a rectangular ROI near the low-contrast circle number 1, and of the same size as the ROI selected from inside the circle;
- ROI is the mean value of the pixel content in the selected ROI of a rectangular ROI inside the circle number 1;
- SD is the corresponding SD for the pixel content in the selected ROIs, inside and outside circle number 1.

$$\mathrm{FOM} = \frac{\mathrm{SNR}^2}{\mathrm{ESAK}} \tag{2}$$

where

- ESAK is the entrance surface air kerma at the point where the x-ray beam axis enters the PMMA.

$$\mathrm{CO} = \frac{[\mathrm{BG} - \mathrm{ROI}]}{\mathrm{BG}}; \tag{3}$$

$$\mathrm{CNR} = \frac{[\mathrm{BG} - \mathrm{ROI}]}{\mathrm{BG}^2}. \tag{4}$$

Some of these image quality parameters have been employed by other authors (Doyle *et al* 2006) in optimizing beam quality for digital chest imaging but using a different definition of FOM incorporating effective dose.

Figure 2 shows the selection of the ROIs for the numerical analysis.

Numerical evaluation was carried out in the first low-contrast circle of the DICOM images obtained for the different operation modes (fluoroscopy and CI) and for the different PMMA thicknesses. The numerical parameter to evaluate changes in the HCSR was the SD of a ROI inside the seventh group (by arbitrary selection) of the central grid, in order of decreasing resolution. The higher the SD the better the HCSR. The reported results for SNR, FOM, CO, CNR and HCSR are mean values and SDs of images numbers 5, 8 and 10 of each series.

Values of cumulative dose displayed (in mGy) at the catheterization room have also been tested for the x-ray system. This quantity is defined at the IEC standard (IEC 2000), and for adult patients, the displayed mGy can be interpreted by cardiologists as a rough indication of the patient skin dose. The DICOM tag (0021, 1007) in the evaluated system is referred to as the 'skin dose accumulation' per CI series or fluoroscopy run in the DICOM Conformance Statement (Axiom 2002). The values reported by the system at the DICOM header have been compared with the experimental ESAK values (see section 2).

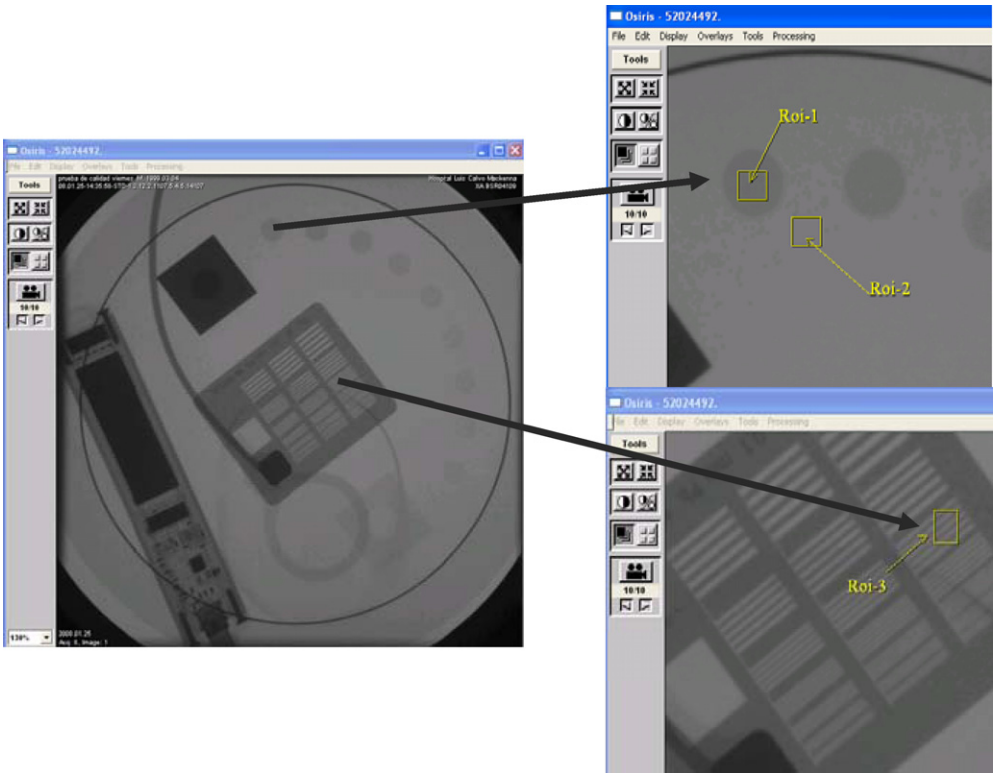

Figure 2. Image of the test object and the ROIs used to measure the different numerical parameters to evaluate image quality.

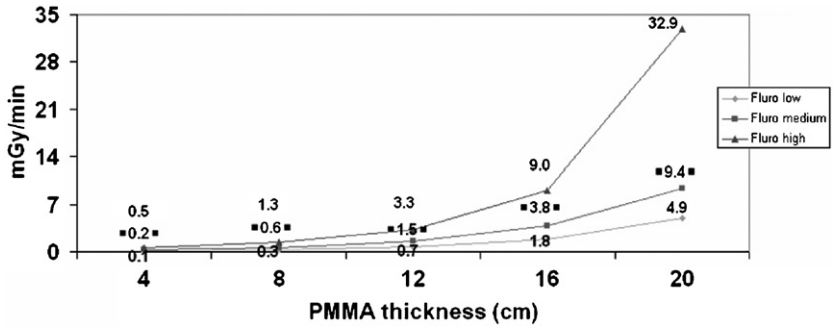

Figure 3. X-ray tube A. PMMA entrance surface air kerma (with BS). Comparison between fluoroscopy low-, medium- and high-dose modes and different PMMA thicknesses. FOV 22 cm. Test object at the isocentre.

3. Results

The ESAK rate and ESAK per frame at the PMMA phantom for 4, 8, 12, 16 and 20 cm and a FOV of 22 cm are presented in figures 3 and 4 for the operations modes used in clinical practice for the evaluated paediatric cardiology x-ray system: fluoroscopy low dose (LD); medium dose (MD); high dose (HD), all with the pulsed rate of 15 frames s^{-1} and CI mode

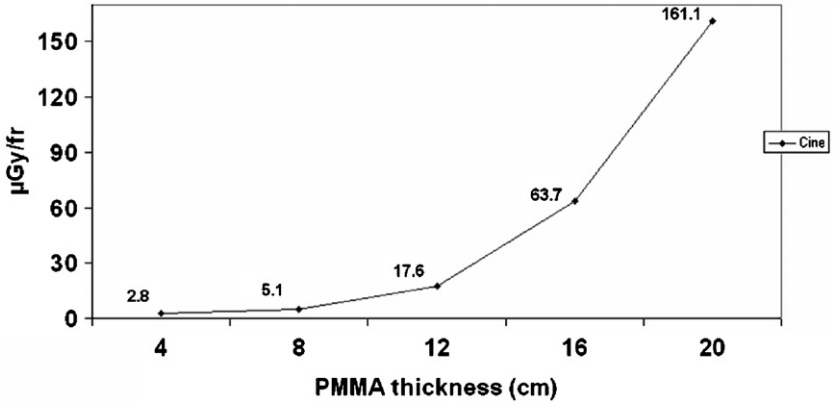

Figure 4. X-ray tube A. PMMA entrance surface air kerma (with BS) per cine frame for different PMMA thicknesses. FOV 22 cm. Test object at the isocentre.

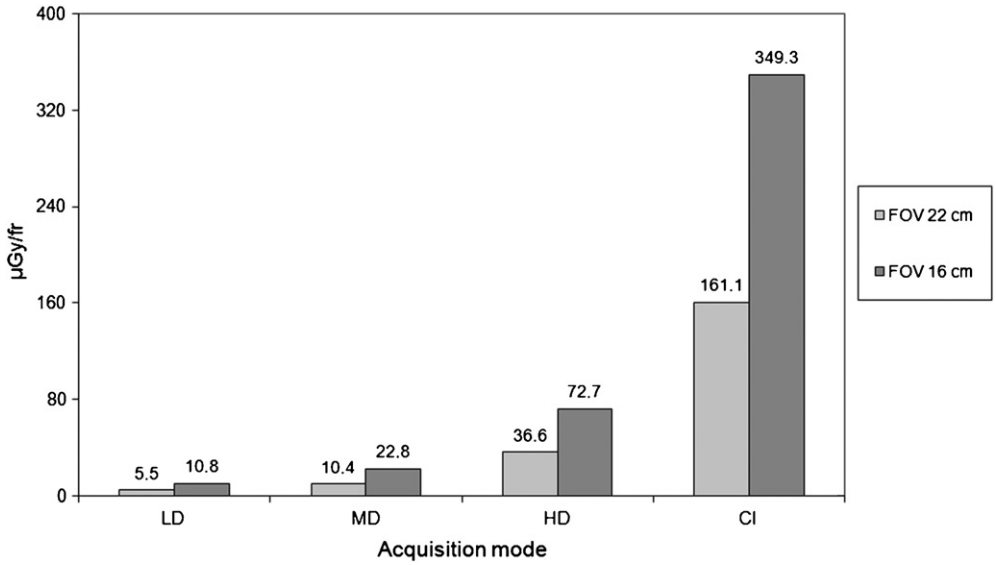

Figure 5. X-ray tube A. ESAK per frame, for 20 cm PMMA and for the different operation modes. Values for the FOVs of 22 and 16 cm are shown.

(typically set at 30 frames s^{-1}). X-ray tube 'A' corresponds to the vertical C-arm. X-ray tube 'B', corresponding to the lateral C-arm, has also been tested and the results are practically the same as for tube A, except that in most of the used projections in clinical practice, the patient table and mattress are not within the beam.

Table 2 shows the numerical values of dose and image quality parameters for the evaluated operation modes and exam protocols together with the most relevant radiographic parameters.

Figure 5 shows the ESAK per frame for different acquisition modes comparing two FOVs for the thickness of 20 cm PMMA. Figure 6 shows the values of SNR and CNR measured for circle 1 in fluoroscopy low and CI modes for different thicknesses of PMMA. Figure 7 shows the values of SNR and CNR measured for circle 1 in all acquisition modes for the thickness

Table 2. Entrance surface air kerma (EASK), signal-to-noise ratio (SNR), figure of merit (FOM), standard deviation for the seventh group in HCSR, contrast (CO) and contrast-to-noise ratio (CNR), tube potential (kVp) and added filter (mmCu) for all the acquisition modes and exam protocol and all PMMA thicknesses used in the study, FOV 22 cm.

PMMA (cm)	Acquisition mode	Exam protocol	ESAK (μGy/frame)	SNR (for circle 1)	FOM $\times$ 1000 (ESAK nGy/frame) (for circle 1)	Standard deviation (for seventh group of HCSR)	CO $\times$ 100 (for circle 1)	CNR $\times$ 10 (for circle 1)	Tube potential (kVp)	Filter (mmCu)
4	LD	New born	0.15	3.70 ± 0.27	93.39	4.75 ± 0.74	7.84 ± 0.65	8.74 ± 7.50	67.0	0.9
4	MD	New born	0.27	3.40 ± 0.34	42.78	4.39 ± 0.67	6.38 ± 0.09	7.04 ± 0.11	75.0	0.9
4	HD	New born	0.56	6.50 ± 0.31	76.49	6.99 ± 0.10	9.61 ± 0.14	10.82 ± 0.15	58.0	0.9
4	CI	New born	2.80	12.60 ± 0.28	56.74	10.35 ± 0.14	17.28 ± 0.15	19.94 ± 0.21	52.0	0.2
8	LD	Infant	0.32	2.70 ± 0.20	22.99	3.34 ± 0.32	5.98 ± 0.41	6.57 ± 0.47	77.0	0.9
8	MD	Infant	0.65	2.67 ± 0.17	11.04	3.15 ± 0.65	5.34 ± 0.15	5.87 ± 0.18	77.0	0.9
8	HD	Infant	1.52	5.98 ± 0.61	23.45	6.46 ± 0.19	9.03 ± 0.28	10.12 ± 0.32	58.0	0.9
8	CI	Infant	5.14	11.56 ± 0.48	25.97	6.11 ± 0.02	10.38 ± 0.11	11.47 ± 0.10	63.0	0.6
12	LD	Child	0.80	2.10 ± 0.09	5.51	3.00 ± 0.55	4.77 ± 0.50	5.20 ± 0.56	77.0	0.9
12	MD	Child	1.60	2.54 ± 0.14	3.86	2.85 ± 0.59	4.89 ± 0.48	5.33 ± 0.52	77.0	0.9
12	HD	Child	3.60	4.87 ± 0.31	6.52	5.08 ± 0.34	7.12 ± 0.15	7.87 ± 0.17	66.0	0.6
12	CI	Child	17.70	11.95 ± 0.63	8.07	5.97 ± 0.10	10.44 ± 0.05	11.43 ± 0.06	67.0	0.3
16	LD	Child	2.10	2.08 ± 0.27	2.08	2.18 ± 0.66	4.97 ± 0.68	5.39 ± 0.75	77.0	0.9
16	MD	Child	4.30	2.46 ± 0.01	1.41	1.91 ± 0.46	5.00 ± 0.08	5.43 ± 0.09	77.0	0.9
16	HD	Child	10.00	4.30 ± 0.47	1.85	3.96 ± 0.14	6.85 ± 0.31	7.52 ± 0.34	66.0	0.6
16	CI	Child	63.70	10.31 ± 0.66	1.67	4.71 ± 0.32	10.25 ± 0.52	11.08 ± 0.58	70.0	0.1
20	LD	Child	5.50	2.07 ± 0.36	0,79	2.09 ± 0.38	4.77 ± 0.43	5.18 ± 0.47	77.0	0.9
20	MD	Child	10.40	2.27 ± 0.13	0.49	1.83 ± 0.10	4.53 ± 0.12	4.87 ± 0.13	90.0	0.6
20	HD	Child	36.60	4.58 ± 0.54	0.57	4.30 ± 0.40	6.44 ± 0.34	7.09 ± 0.38	68.0	0.3
20	CI	Child	161.10	9.50 ± 0.55	0.56	3.53 ± 0.27	8.82 ± 0.05	9.48 ± 0.05	74.0	0.1

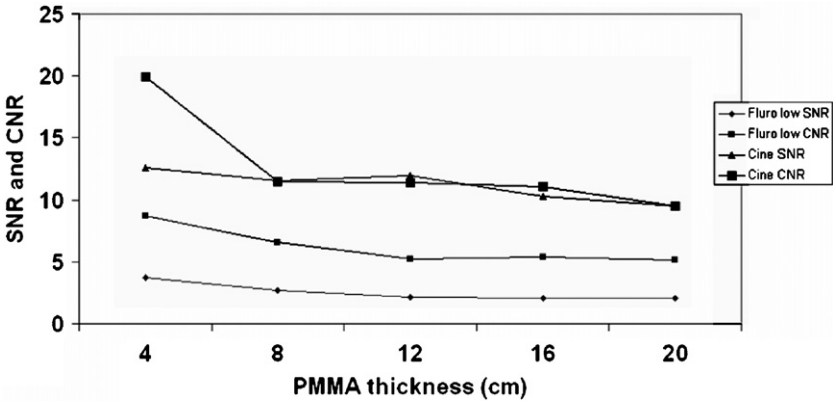

Figure 6. X-ray tube A. Signal-to-noise ratio (SNR) and contrast-to-noise ratio (CNR). Fluoroscopy low and cine modes and different PMMA thicknesses. FOV 22 cm.

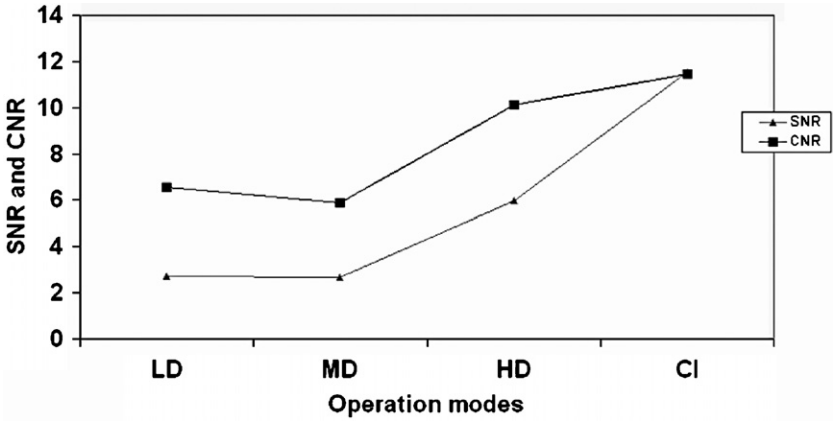

Figure 7. X-ray tube A. Signal-to-noise ratio (SNR) and contrast-to-noise ratio (CNR). For all operation modes and 8 cm PMMA thickness. FOV 22 cm.

of 8 cm PMMA. Figure 8 shows the tendency (for fluoroscopy low and high modes) of the numerical parameters (SD of a ROI selected in group 7 of the HCSR bars) used to measure the degradation of HCSR when the thickness of the phantom increases.

Table 3 shows an example of the results using the FOV of 16 cm. Table 4 presents some examples of the PMMA ESAK values measured over the patient table with the calibrated solid-state detector, for CI mode, and the corresponding figures recorded by the x-ray system in the DICOM header.

4. Discussion

4.1. Dose

ESAK for low fluoroscopy mode ranges from 0.15 to 5.50 μGy/frame, when the PMMA thickness is increased from 4 to 20 cm. Other fluoroscopy modes have similar variations (see table 2). For CI, these values range from 2.80 to 161.10 μGy/frame. The increase factors due

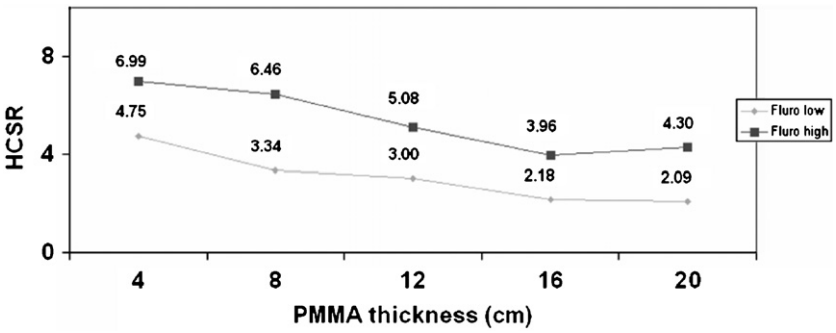

Figure 8. X-ray tube A. High-contrast spatial resolution-related parameter (HCSR). Fluoroscopy low and high modes and different PMMA thicknesses. FOV 22 cm.

Table 3. Entrance surface air kerma (ESAK) and standard deviation (SD) in HCSR for the FOV 16 cm.

PMMA (cm)	Acquisition mode	Exam protocol	ESAK (μGy/frame)	SD for seventh group in HCSR
20	LD	Child	10.81	2.83 ± 0.21
20	MD	Child	22.81	3.19 ± 0.17
20	HD	Child	72.73	5.08 ± 0.22
20	CI	Child	349.31	4.23 ± 0.18

Table 4. Examples of ESAK measured values (including BS and table attenuation) during the experiment and the corresponding figures transferred by the x-ray system to the DICOM header (incident air kerma values at the interventional reference point), tube potential (kVp) and added filter (mmCu) for cine acquisition modes and for all exam protocols and all PMMA thicknesses used in the study, FOV 22 cm.

PMMA (cm)	Acquisition mode	Exam protocol	Measured ESAK (mGy/frame)	Dose value transferred to the DICOM header (mGy/frame)	Difference (%)	Tube potential (kVp)	Filter (mmCu)
4	CI	New born	2.80	5.03	+44.0	52.0	0.2
8	CI	Infant	5.14	8.47	+39.3	63.0	0.6
12	CI	Child	17.68	26.51	+33.3	67.0	0.3
16	CI	Child	63.74	94.78	+32.8	70.0	0.1
20	CI	Child	161.11	214.35	+24.8	74.0	0.1

to patient size are around 40 and 60 for fluoroscopy and CI modes, respectively. Figures 3 and 4 show the increases in ESAK with the phantom thickness for fluoroscopy and CI modes. Roughly, an increase in the thickness by 4 cm involves increases in ESAK by a factor of around 3. Another important aspect to be considered by cardiologists is the increase in the ESAK/frame by factors of between 20 and 30 when comparing CI with LD fluoroscopy frames. This system allows the archiving of fluoroscopy runs in DICOM format and if high image quality is not required, a fluoroscopy run should be considered as an alternative to document part of the procedure. Figure 5 shows that increases in ESAK per frame when electronic magnification is applied (FOVs from 22 to 16 cm) move from 96 to 119%. It is

important that these increase factors in dose be known to cardiologists when they use different C-arm angulations, operation modes, electronic magnification and different patient sizes.

4.2. Image quality

For the same thickness, the increase in dose per frame should always involve better image quality and if the system is properly adjusted, image quality should be roughly maintained when the thickness of the phantom is increased (with a reasonable increase in dose).

The SNR compares the level of a desired 'signal' in the image (such as an artery or a stent) to the level of background (the tissue around the artery or the stent) but takes into account the statistical quantum fluctuation (especially important when low fluoroscopy modes are used). The higher the SNR, the better the visualization of low CO objects. The CNR refers to the ability of an imaging mode to distinguish between various contrasts of an acquired image and the inherent noise in the image. The higher the CNS, the more the capacity to distinguish a guide wire or a stent inside a vessel. When images have low quantum noise (e.g. CI modes) both parameters (SNR and CNR) are similar (as can be seen in figure 7). For LD modes (with noisy images) the SNR is a better numerical parameter to identify image quality.

The SNR for low fluoroscopy mode moves from 3.70 (for 4 cm PMMA) to 2.07 (for 20 cm PMMA) and from 12.60 to 9.50 for CI mode (table 2). The increase in the values of dose per frame and the change in radiographic techniques cannot maintain the same SNR for thicker patients, but the slight reduction in the SNR is reasonable (figure 6). Values of kV and copper filter (see table 2) allow understanding of the logic applied by the x-ray system to the different protocols. Figure 7 shows the variation in SNR and CNR when moving from the LD, MD and HD fluoroscopy to CI modes. Note that image quality clearly improves when dose is increased except for MD fluoroscopy, suggesting that the setting of this mode should be reconsidered. This apparently abnormal setting of the MD fluoroscopy is also evident when looking at the values of the FOM (table 2) in comparison to the other fluoroscopy modes.

The parameter FOM has previously been used by other authors (Zamenhof 1982, Gagne *et al* 2003) for the optimization of signal detectability in digital imaging; it allows the relation of the quality of an image and the dose per frame that was necessary to obtain this image. In our case, the FOM shows, except for 4 cm PMMA, values with maximum differences of around a factor of 2, meaning a well-balanced compromise between the increase in dose per frame and image quality. Of course, a decreasing tendency is evident with increasing PMMA thickness.

Numerical evaluation of the HCSR shows an increase in fluoroscopy HD and CI (for the same PMMA thickness) due to the increase in the dose per frame values and the corresponding low noise. When the phantom thickness is increased, this numerical parameter decreases accordingly due to the influence of scatter radiation (see table 2). But these changes are not fully apparent visually. The numerical analysis (figure 8) is the means used to appreciate the changes in HCSR.

The electronic magnification, when changing the FOV from 22 to 16 cm, clearly improves the HCSR (table 3), but also increases the entrance dose by a factor of 1.9 for CI in the evaluated system. This increase in ESAK, when known to cardiologists, should allow them to consider the use (in some cases) of numerical magnification instead of electronic magnification.

4.3. Use of the cumulative dose display for paediatrics

Cumulative dose values presented in the catheterization room by the x-ray system and transferred to the DICOM header of the series are reported in table 4. The greatest differences

are for the thickness of 4 cm of PMMA (44%). The cumulative dose is calculated at 15 cm down from the isocentre, and for a thickness of 4 cm the phantom entrance is only around 2 cm down from the isocentre. Thus, the mGy value displayed by the system is significantly higher than the real ESAK dose values (typically considered by cardiologists as patient skin dose). The geometry of the system and the quality of the x-ray beam are the main factors influencing these differences between the displayed and the real values. For paediatric patients, the skin is typically more distant from the x-ray source than the interventional reference point and receives a smaller dose than the one calculated at that point. Other factors influencing the attenuation in the table supporting the patient are kV and copper filter, resulting in the differences shown in table 4. For adult patients, the displayed cumulative dose is very close to the skin dose, because the attenuation of the table is compensated for with the increase of the BS factor (Vano *et al* 2005), and the typical position of the patient skin (for normal size patients) is around 15 cm down from the isocentre (as defined by IEC) (IEC 2000).

5. Conclusions

The characterization in dose and image quality for a biplane paediatric system has been made for phantom thicknesses ranging from 4 to 20 cm of PMMA, measuring the dose per frame values for fluoroscopy and cine modes and computing different numerical parameters to evaluate low contrast detectability and HCSR. The SNR, CO, CNR and FOM and SD for HCSR for the different image acquisition modes have been reported to verify the appropriate setting of the system. Numerical values, especially increases in dose per frame when increasing phantom thickness and applying electronic magnification, should help the cardiologist in the good management of patient dose. Knowledge of dose values and the obtained image quality for the different operation modes is essential to optimize operational procedures. The use (and archiving) of fluoroscopy instead of CI runs is a good option when high image quality is not necessary (meaning roughly a saving in dose of a factor of 20). The relation between values of the cumulative dose displayed by the system and patient entrance doses has also been evaluated for paediatric thicknesses. Some suggestions to improve the present setting of the x-ray system have also been obtained.

Acknowledgments

The present work has been carried out as part of the program ‘Strengthening Radiological Protection of Patients and in Medical Exposures (TSA3), RLA/9/057’ of the International Atomic Energy Agency (IAEA). One of the authors (EV) also acknowledges the support of the Spanish grant FIS2006-08186 (Ministry of Education and Science).

References

Axiom 2002 Axiom Artis VA20F/VA21x/VA22x. DICOM Conformance statement. Rev. 02 (10 October 2002). Release 10.02.Siemens AG. Wittelsbacher Platz 2, D-80333 Munich, Germany. Available at http://www.medical.siemens.com/siemens/de_DE/rg_marcom_F BAs/files/brochures/DICOM/ax/ARTIS_DCS_VA22B_02.pdf (last accessed 27 April 2008)

Bacher K, Bogaert E, Lapere R, De Wolf D and Thierens H 2005 Patient-specific dose and radiation risk estimation in pediatric cardiac catheterization *Circulation* **111** 83–9

Balter S, Miller D L, Vano E, Ortiz Lopez P, Bernanrdi G, Cotelo E, Faulkner K, Nowotny R, Padovani R and Ramirez A 2008 A pilot study exploring the possibility of establishing guidance levels in x-ray directed international procedures *Med. Phys.* **35** 673–80

Doyle P, Martin C J and Gentle D 2006 Application of contrast-to-noise ratio in optimizing beam quality for digital chest radiography: comparison of experimental measurements and theoretical simulations *Phys. Med. Biol.* **51** 2953–70

EC 1997 European Commission, Council Directive 97/43/EURATOM of 30 June 1997 on health protection of individuals against the dangers of ionizing radiation in relation to medical exposure *Off. J. Eur. Commun.* L **180** 22–7

Faulkner K 2001 Introduction to constancy check protocols in fluoroscopic systems *Radiat. Prot. Dosim.* **94** 65–8

Faulkner K, Malone J, Vano E, Padovani R, Busch H P, Zoetelief J H and Bosmans H 2008 The SENTINEL Project *Radiat. Prot. Dosim.* published online doi: 10.1093/rpd/ncn019

Gagne R M, Boswell J S and Myers K J 2003 Signal detectability in digital radiography: spatial domain figures of merit *Med. Phys.* **30** 2180–93

IAEA 2007 Radiological protection of patients and in medical exposures (TSA3) *ARCAL project RLA/9/057* International Atomic Energy Agency, http://www-tc.iaea.org/tcweb/projectinfo/projectinfo_body.asp (last access 27 April 2008)

ICRU 2005 Patient Dosimetry for X Rays Used in Medical Imaging *ICRU Report 74* (Bethesda, MD: International Commission on Radiological Units and Measurements)

IEC 2000 Medical electrical equipment: Part 2–43. Particular requirements for the safety of x-ray equipment for interventional procedures International Electrotechnical Commission (IEC) 60601-2-43, 1st edn 2000–06 (Geneva, Switzerland: International Electrotechnical Commission)

Martinez L C, Vano E, Gutierrez F, Rodriguez C, Gilarranz R and Manzanas M J 2007 Patient doses from fluoroscopically guided cardiac procedures in pediatrics *Phys. Med. Biol.* **52** 4749–59

Massoumzadeh P, Rudin S and Bednarek D 1998 Filter material selection for region of interest radiologic imaging *Med. Phys.* **25** 161–71

Rassow J, Schmaltz A A, Hentrich F and Streffer C 2000 Effective doses to patients from paediatric cardiac catheterization *Br. J. Radiol.* **73** 172–83

Siemens 2008 http://cardiology.usa.siemens.com/products-and-it-systems/cardiology-products/interventional-cardiology/artis-bc/technical-specifications.aspx (last accessed 13 June 2008)

Simon R, Vano R, Prieto C, Fernandez J M, Ordiales J M and Martinez D 2008 Criteria to optimise a dynamic flat detector system used for interventional radiology *Radiat. Prot. Dosim.* published online doi: 10.1093/rpd/ncn027

Tsapaki V, Kottou S, Kollaros N, Dafnomili P, Koutelou M, Vano E and Neofotistou V 2004a Comparison of a conventional and a flat-panel digital system in interventional cardiology procedures *Br. J. Radiol.* **77** 562–7

Tsapaki V, Kottou S, Kollaros N, Dafnomili P, Kyriakidis Z and Neofotistou V 2004b Dose performance evaluation of a charge coupled device and a flat-panel digital fluoroscopy system recently installed in an interventional cardiology laboratory *Radiat. Prot. Dosim.* **111** 297–304

UNSCEAR 2000 United Nations Scientific Committee on Effects of Atomic Radiations Source and Effects of Ionizing Radiation *Report to the general assembly with scientific,* Annexes 3. Volume I. Sources. United Nations, New York

Vano E, Geiger B, Schreiner A, Back C and Beissel J 2005 Dynamic flat panel detector versus image intensifier in cardiac imaging: dose and image quality *Phys. Med. Biol.* **50** 5731–42

Wagner L K 2006 Minimizing radiation injury and neoplastic effects during pediatric fluoroscopy: what should we know? *Pediatr. Radiol.* **36** 141–5

Zamenhof G 1982 The optimization of signal detectability in digital fluoroscopy *Med. Phys.* **9** 688–94